Molecular Simulation of Permeation of Small Penetrants through Membranes. 1. Diffusion Coefficients

Yoshinori Tamai[*,†]

Tokyo Research Center, Tosoh Corporation, 2743-1, Hayakawa, Ayase, Kanagawa 252, Japan

Hideki Tanaka and Koichiro Nakanishi

Department of Polymer Chemistry, Kyoto University, Kyoto 606-01, Japan

Received February 18, 1994; Revised Manuscript Received May 23, 1994[⊕]

ABSTRACT: Molecular dynamics simulations have been carried out in order to examine the mechanism of diffusion of small penetrants in amorphous polymer membranes. Diffusion processes of methane, water, and ethanol in poly(dimethylsiloxane) (PDMS) and in polyethylene (PE) were investigated. Pure liquid water and ethanol were also simulated. The insertion probabilities $P(R)$ of hard-sphere atoms of radius R into the polymers and the liquids were calculated. The free volume fraction, $P(0)$, of PDMS is large and the insertion probability of a finite size atom into PDMS is widely distributed compared with the other polymers and liquids. Simulations of 5 ns were performed for PDMS and in PE with a penetrant species, methane. The diffusion of methane in the polymer matrix exhibits anomalous (non-Einstein) behavior for time scales of 1 and 0.3 ns in PDMS and PE, respectively. Aggregates of water and ethanol are found to be formed in PDMS. Diffusion coefficients of water and ethanol in PDMS are reduced by more than 1 order of magnitude due to the aggregation. The calculated diffusion coefficients of the nonaggregated penetrants in PDMS and in the pure liquids agree well with the experimental values.

Introduction

Poly(dimethylsiloxane) (PDMS) is the well-known membrane which separates ethanol from the aqueous solution by pervaporation. Pervaporation[1] is a method of separating the mixture of liquids by membranes. The components of the liquid mixture are supplied on the feed side of the membrane and diffuse to the permeate side of the membrane, where pressure is diminished, leaving the membrane as vapor. The separation process is accounted for by the sorption–diffusion model.

The sorption–diffusion model describes permeation of small molecules through a nonporous polymer membrane. Sorption of small molecules on the surface of a membrane causes a concentration gradient in the membrane, and the gradient causes diffusion of the molecules. The permeation rate P of small penetrants depends on solubility and diffusivity and is expressed by

$$P = DS \tag{1}$$

where D is the diffusion coefficient and S is the solubility of penetrants. When considering the separation of the mixture of two components, the separation factor of component 1 is expressed by

$$\alpha_1 = P_1/P_2 \tag{2}$$

where P_1 and P_2 are permeation rates of components 1 and 2, respectively, which are calculated from the diffusion coefficients and the solubilities of components 1 and 2.

It is useful for the design of functional separation membranes to predict the solubility and diffusion coefficient using a molecular simulation technique. Diffusion coefficients of small penetrant molecules in an amorphous polymer matrix can be calculated by a molecular dynamics (MD) simulation. Solubilities can be calculated by the Widom test particle insertion method.[2]

The diffusion coefficients of small penetrant molecules in amorphous polymer matrices have been calculated from MD simulations.[3-11] All these calculations were performed for nonpolar small molecules: helium, methane, oxygen, etc. In the early works the calculated diffusion coefficients of small penetrants in polyethylene (PE), polyisobutylene (PIB), and atactic polypropylene (a-PP) were 10–100 times higher than the experimental values. Müller-Plathe et al.[7] attributed those deviations to the united atom approximation. They calculated the diffusion coefficients of oxygen in PIB using the all-atom force field with explicit hydrogen atoms and obtained the value which is close to the experimental value. Pant et al.[10,11] calculated the diffusion coefficients of methane in PE and PIB using the anisotropic united atom (AUA) potential, in which off-center Lennard-Jones potentials were used for the nonbonded interactions, and they obtained values close to the experimental ones. On the other hand, Sok et al.[5] obtained a value of the diffusion coefficient of methane in PDMS close to the experimental one, in spite of the united atom approximation. The discrepancy between experimental and calculated diffusion coefficients by use of the united atom approximation depends largely on the size of the penetrants, as discussed by Müller-Plathe; the larger the penetrant is, the smaller the discrepancy is.

For a simple liquid, the diffusion coefficient can be calculated by relatively short time runs of the MD simulation. For a small molecule in a polymer matrix, however, very long time runs of the MD simulation are required. Müller-Plathe et al.[8] performed several nanoseconds of MD simulation for He and O_2 in PIB. The diffusion of He and O_2 through the polymer matrix exhibits anomalous (non-Einstein) behavior for time scales of at least 0.1 and 6 ns for He and O_2, respectively. Gusev et al.[12,13] calculated the diffusion coefficients of light gases in rubbery PIB and glassy Bisphenol A polycarbonate (PC) by the new transition-state theory which takes atomistic microstructures into consideration using the information on the mobility of the host matrix, which was calculated

[†] Present address: Department of Polymer Chemistry, Kyoto University, Kyoto 606-01, Japan.

[⊕] Abstract published in *Advance ACS Abstracts*, July 1, 1994.

0024-9297/94/2227-4498$04.50/0

from short-time-scale MD runs. Because the mobility of the polymer chains is very low in the glassy state, the diffusion coefficients of Ar, O_2, and N_2 in PC are very small; it takes a very long time scale ($\sim 1\ \mu s$) to exhibit the normal diffusion behavior.

The diffusion coefficient is dependent on the free volume and its distribution. Shah et al.[14] calculated the available free volume distribution for penetrants in polymers using a Monte Carlo integration method where they measured the diameter of the largest hard sphere which could be located at a randomly chosen point in the polymers. Arizzi et al.[15] divided the structures of a-PP and PC into tetrahedral interstices using Delaunay tessellation and calculated the fraction of the interstices which are accessible for small penetrants. They also analyzed the connectivity of the interstices. Greenfield et al.[16] reported a similar analysis for a-PP. Misra et al.[17] divided the unit cell of polybutadiene into small cubes and calculated the accessible volume fraction for small penetrants and also analyzed the cluster of the accessible cubes.

In this study, we used the united atom approximation and performed 2–5 ns of MD simulations. We calculated the diffusion coefficients of methane, water, and ethanol in PDMS by the MD simulation in order to examine a permeative mechanism of small molecules in the PDMS membrane. These systems are quite different from the previous works, because we consider larger penetrants and penetrants which can form hydrogen bonds. For comparison, we calculated diffusion coefficients of methane, water, and ethanol in PE and those of pure liquid water and ethanol. We also calculated the insertion probabilities[18] $P(R)$ of hard-sphere atoms of radius R into the polymers and the liquids. We will evaluate the solubilities by the Widom test particle insertion method in an accompanying paper.

Model and Simulation Details

Simulation Program. We coded the PAMPS (Molecular Simulation *P*rograms for *A*nalysis of *M*ixtures of *P*olymers and *S*mall Molecules): a general program package for molecular simulation of the mixtures of polymers and/or small molecules. All calculations were performed on CRAY Y-MP2E using this program package.

Model. The PDMS sample is modeled as $CH_3[-Si(CH_3)_2O-]_{30}Si(CH_3)_3$ and the PE sample is modeled as $CH_3[-CH_2-]_{120}CH_3$. There are no cross-links and branches. Simulations were carried out for the systems containing five polymer chains in cubic periodic boxes. The simulations for pure liquid water and ethanol were also carried out for the systems containing 216 and 128 molecules, respectively, in cubic periodic boxes. The experimental densities at 300 K were used, i.e., 0.95, 0.855, 0.9965, and 0.7851 g/cm^3 for PDMS,[5] PE,[10,21] water,[19] and ethanol (25 °C),[20] respectively. PE is a semicrystalline polymer, and the density is varied with crystallinity. Since diffusion of small penetrants takes place only in an amorphous region, the density of the amorphous fraction was used for PE in the present simulation. The density of PDMS varies with the degree of polymerization and cross-link. We used the same density as the study of Sok et al. to compare the results.

Potential Functions. The OPLS (optimized potential for liquid simulations) models have been developed by Jorgensen et al.[20,22] for water and organic liquids. The OPLS describes intermolecular interaction effectively and reproduces experimental thermodynamic properties by molecular simulation. To simulate mixtures of polypeptide and water, the OPLS force field was merged into the AMBER,[23] i.e., the OPLS for intermolecular potential functions and the AMBER for intramolecular ones (AMBER/OPLS).[24] They performed energy minimization for crystals of polypeptide with water and obtained reasonable results. In this study, we use the AMBER/OPLS except for PDMS and water. The GROMOS[5] force field is used for PDMS and the SPC/E[25] for water. All CH_4, CH_3-, and $-CH_2-$ groups are treated as united atoms.

The bond lengths are constrained to the equilibrium bond lengths r_0 by the SHAKE[26] algorithm. The bond angles of polymers and ethanol are subjected to the harmonic potential given by

$$V(\theta) = k_\theta(\theta - \theta_0)^2 \tag{3}$$

where θ_0 is the equilibrium bond angle and k_θ is the force constant. The bond angles of water are constrained by the SHAKE algorithm. The dihedral angle rotations are described as

$$V(\phi) = k_\phi[1 + \cos(n\phi - \delta)] \tag{4}$$

where k_ϕ is the force constant, n is the multiplicity factor, and δ is the phase shift. The dihedral angle potential adopted for ethanol is taken from the OPLS potential model

$$V(\phi) = V_0 + \frac{1}{2}V_1(1 + \cos\phi) + \frac{1}{2}V_2(1 - \cos 2\phi) + \frac{1}{2}V_3(1 + \cos 3\phi) \tag{5}$$

where $V_i (i=0,1,2,3)$ are the force constants. This is the potential function of the OPLS. The nonbonded interactions are described as

$$V(r) = \frac{A_{ij}}{r^{12}} - \frac{C_{ij}}{r^6} + \frac{q_i q_j}{4\pi\epsilon_0 r} \tag{6}$$

where q_i is the charge of atom i, and ϵ_0 is the dielectric constant in vacuum. Standard combining rules are used for the Lennard-Jones interactions such that $A_{ij} = (A_{ii}A_{jj})^{1/2}$ and $C_{ij} = (C_{ii}C_{jj})^{1/2}$, where A_{ii} and C_{ii} are expressed in terms of Lennard-Jones parameters as $A_{ii} = 4\epsilon_i\sigma_i^{12}$ and $C_{ii} = 4\epsilon_i\sigma_i^6$. The 1,4 nonbonded interactions are scaled from the normal nonbonded interaction by dividing the Lennard-Jones terms of PE by factors 8.0 and the Coulombic terms by factors 2.0.[24] All potential parameters used in the simulations are summarized in Table 1.

Because the force constant of the bond angle Si–O–Si of PDMS is small and the equilibrium bond angle is large (144°), the probability that the bond angle goes across $\theta = 180°$ cannot be neglected at high temperature. Since the derivative of the potential functions with respect to the atom positions is not continuous at $\theta = 180°$, an energy jump occurs when the bond angle goes across $\theta = 180°$. To circumvent this energy jump, we added the auxiliary term

$$\begin{aligned} V(\theta) &= V_0(\theta), \quad \theta \le \theta_s \\ &= V_0(\theta) + k_s(\theta - \theta_s)^2, \quad \theta > \theta_s \end{aligned} \tag{7}$$

where $V_0(\theta)$ is the original potential function. We used 1.0×10^{-4} kJ/mol and 165° for k_s and θ_s, respectively. This term prevented the energy jump and did not change the bond angle distribution at 300 K.

Simulation of Amorphous PDMS. Using the modified self-avoiding random walk,[5,27] five polymer chains were

Table 1. Potential Parameters[a]

bond	r_0	bond	r_0
Si–O	1.600	O–H (water)	1.000
Si–CH_3	1.880	O–H (ethanol)	0.960
CH_2–CH_2	1.526	O–CH_2	1.425
CH_2–CH_3	1.526		

angle	k_θ	θ_0	angle	k_θ	θ_0
Si–O–Si	59.0	144.0	CH_2–CH_2–CH_3[b]	263.8	112.4
O–Si–O	395.7	109.5	H–O–H	c	109.5
O–Si–CH_3	209.3	109.5	H–O–CH_2	230.3	108.5
CH_3–Si–CH_3	209.3	109.5	O–CH_2–CH_3	334.9	109.5
CH_2–CH_2–CH_2	263.8	112.4			

dihedral	k_ϕ	n	δ
Si–O–Si–O	3.77	3	0
Si–O–Si–CH_3	3.77	3	0
CH_2–CH_2–CH_2–CH_2	8.37	3	0
CH_2–CH_2–CH_2–CH_3	8.37	3	0

dihedral (ethanol)	V_0	V_1	V_2	V_3
H–O–CH_2–CH_3	0.0	3.492	−0.486	3.128

nonbonded	ϵ	σ	q	m
CH_4	1.2309	3.730	0.0	16.0430
CH_3 (PDMS)	0.7532	3.786	0.0	15.0350
CH_3 (PE)	0.7327	3.905	0.0	15.0350
CH_3 (ethanol)	0.7327	3.905	0.0	15.0350
CH_2 (PE)	0.4940	3.905	0.0	14.0270
CH_2 (ethanol)	0.4940	3.905	0.265	14.0270
Si	2.4480	3.385	0.300	28.0800
O (PDMS)	0.8493	2.955	−0.300	15.9990
O (water)	0.6502	3.1656	−0.8476	15.9994
O (ethanol)	0.7118	3.070	−0.700	15.9994
H (water)	0.0	0.0	0.4238	1.0080
H (ethanol)	0.0	0.0	0.435	1.0080

[a] Energies are in kJ/mol, distances in Å, and angles in rad (θ_0 in deg). [b] The parameter for CH_2–CH_2–CH_3 is not in the AMBER. The same parameter as for CH_2–CH_2–CH_2 is used. [c] The bond angles of H–O–H of water are constrained.

packed into a unit cell under the periodic boundary condition at a density of 0.5 g/cm^3. In this method a chain is built up site by site with fixed bond lengths and bond angles and with randomly generated dihedral angles. In this stage, nonbonded potentials were modeled by the soft core type repulsive potentials in the same manner as Sok et al.[5] The 1,4-interaction energy of a main chain was described as

$$V(\phi) = k_\phi(1 + \cos 3\phi) + V_{RIS} \quad (8)$$

where V_{RIS} is the first-order interaction energy of the rotational isomeric states (RIS) model,[28] and no 1,4 nonbonded interaction was included in this term. In this study, we used the RIS parameters of both Bahar, Zuniga, Dodge, and Mattice (BZDM)[30,31] and Flory, Crescenzi, and Mark (FCM).[29] The results from both parameters were compared.

A new position (dihedral angle ϕ) was generated, which was either accepted or rejected by the Monte Carlo method similar to the Metropolis scheme, thereby evaluating the potential energy using both sets of RIS parameters. To set a head group of the chain, the head group, which consists of the first three atoms of the chain, is settled in the unit cell at a random position with a random Euler angle, and then the position is accepted or rejected in the same manner. After the position of the head group is accepted, dihedral angles for the atoms of the subsequent chain are generated successively. (For small molecules, only the first step of the method is applied.) After the packing of chains was completed, excess overlaps of atoms were eliminated by 1000 steps of the steepest-descent energy minimization using the potential without the Coulombic term and by subsequent 1000 steps of energy minimization with the full potential. Then, MD simulation was performed for a full potential system. The volume of the unit cell was decreased by a small amount at every time step. After reaching the experimental density, the usual MD simulation was performed, where the box length was 27.24 Å.

The equations of motion were solved using the Verlet algorithm[32] with a time step of 5 fs under the constant NVE condition. The Lennard-Jones terms of the potential were cut off at 10 Å. Long-range Coulombic interactions were handled by the Ewald sum method.[33] The Verlet neighbor list[33] was used with automatic updating of the list. Temperature scalings were imposed every 5 ps to prevent creep of temperature in long time simulation. The system was stable during the whole simulation step, and the average value of the scaling factors of velocities is nearly unity. MD simulation was performed for 625 ps at 300 K, for 150 ps at 1000 K to relax the structure, and then for 625 ps at 300 K. The trajectory of the last 500 ps was used for analysis of the amorphous structure.

Simulation of Amorphous PE. The amorphous structure of PE was generated by the same method as given above. The description of the 1,4-interaction energy of a main chain is slightly different. The soft core type repulsive potentials were used instead of V_{RIS} in eq 8. After 1000 steps of energy minimization, MD simulation was performed with gradual compression of the unit cell until the experimental density is achieved. The final box length was 25.46 Å. MD simulation was performed for 250 ps at 300 K, for 150 ps at 1000 K, and then for 1100 ps at 300 K. The trajectory of the last 500 ps was used for analysis of the amorphous structure.

Simulation of Pure Liquids. For the simulations of pure liquid water and ethanol, 216 and 128 molecules, respectively, were confined in periodic boxes at the experimental densities by applying the first step of the modified self-avoiding random walk. The box lengths were 18.65 and 23.19 Å for water and ethanol, respectively. After 2000 steps of energy minimization, MD simulations were performed under the constant NVT condition. The NVT method by Nosé[34] was utilized. The iterative method of Ferrario et al.[35] was used to integrate the equations of motion of the NVT ensemble using the Verlet algorithm and the SHAKE method. The inertial parameter for the extra variable was 7000 amu Å^2, which gave a frequency of about 1 ps for the fluctuation of the extra variable. This time scale is the same as that in the study of Palmer et al.,[36] where several dynamical properties were discussed. A time step of 0.5 fs was used. The Lennard-Jones terms were cut off at 9 and 10 Å for water and ethanol, respectively. The Ewald sum method and the Verlet neighbor list were used. After 150 ps of MD runs to equilibrate the systems, a trajectory of 50 ps was sampled for water and of 100 ps for ethanol.

Diffusion of Small Penetrants in Polymers. One or five penetrant molecules were inserted into the polymer structure using the modified self-avoiding random walk. The Lennard-Jones potentials were used for nonbonded interaction at this stage. For the system which contains five penetrant molecules, the initial positions of five penetrants were determined so that an arbitrarily chosen penetrant was separated from any other penetrants by at least 10 Å to disperse the penetrant molecules in the unit cell. MD simulations were performed with writing out coordinates of atoms on the files. The sampling time was 500 ps for the short time runs and 2000 or 5000 ps for the

Table 2. Sampling Times and Time Steps for Various MD Simulations

matrix	penetrant	sampling (ps)	time step (fs)
	Pure Polymers and Liquids		
PDMS		500	5
PE		500	5
water		50	0.5
ethanol		100	0.5
	Penetrants in PDMS (Long Time Runs)		
PDMS	methane × 5	5000	5
PDMS	water × 1	2000	2
PDMS	water × 5	2000	2
PDMS	ethanol × 1	2000	2
PDMS	ethanol × 5	2000	2
	Penetrants in PDMS (Short Time Runs)		
PDMS	water × 5	500	1
PDMS	ethanol × 5	500	1
	Penetrants in PE		
PE	methane × 5	5000	5
PE	water × 1	2000	2
PE	ethanol × 1	2000	2

long time runs. A time step of 1 fs was used for short time runs. For the long time runs, a time step of 5 fs was used for the methane/polymer system, and a time step of 2 fs was used for the water/polymer and ethanol/polymer systems. The time step of 2 fs for water is rather long compared with the simulation of liquid water and ethanol. Since we are interested mainly in translational motion and long time behavior in the present simulation, we used these time steps. The MD methods were the same as those used for PDMS. The simulated systems and conditions are summarized in Table 2.

Diffusion coefficients were calculated from the least-square fits of the mean-square displacements of the centers of mass of the penetrant molecules averaged over all possible time origins as

$$D = \lim_{t\to\infty} \frac{1}{6t}\langle[\mathbf{R}(t) - \mathbf{R}(0)]^2\rangle \tag{9}$$

where $\mathbf{R}(t)$ is a position of the center of mass of a penetrant at time t and $\langle\ \rangle$ means an ensemble average.

Insertion Probabilities. We calculated the insertion probability $P(R)$, which is defined as the probability that a hard-sphere solute of radius R could be located at an arbitrary point in the matrix without overlap with the van der Waals volume of any matrix molecule.[18] $P(R)$ is related to the free volume fraction and its distribution. We also calculated its derivative

$$P_m(R) = -dP(R)/dR \tag{10}$$

which is the probability that the largest hard-sphere solute that could be inserted at an arbitrary point would have a radius within dR of R.

Each atom of the matrix was modeled as a hard sphere of radius $\sigma/2$, where σ means the Lennard-Jones size parameter. The histogram was constructed with regard to the minimum distances from each grid point of 100 × 100 × 100 on the unit cell to the surfaces of the hard sphere of the matrix. This histogram leads to $P_m(R)$ by normalization, and $P_m(R)$ was integrated to

$$P(R) = \int_R^\infty P_m(R')\, dR' \tag{11}$$

Time dependence and time averages of $P(R)$ and $P_m(R)$ were calculated over the 250–1000 coordinates of trajectories.

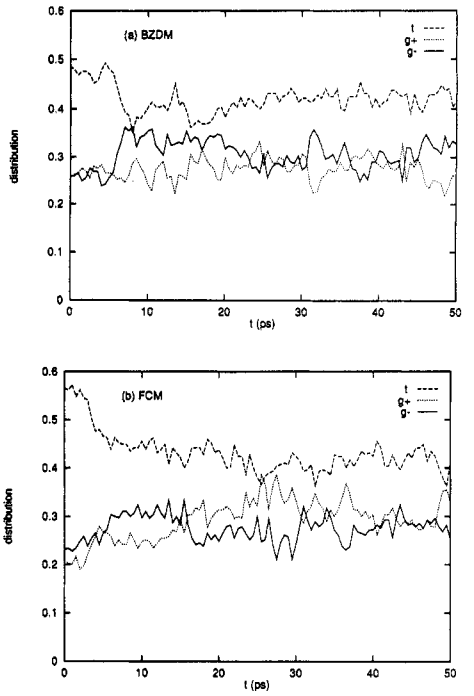

Figure 1. Time dependence of the dihedral angle distribution of Si–O–Si–O of PDMS at 1000 K. The initial structures were generated using (a) the BZDM RIS parameters and (b) the FCM.

Results and Discussion

Structure of Amorphous PDMS. We generated two different initial structures using different RIS parameters: the BZDM and the FCM. These initial structures give different profiles of the insertion probability $P(R)$ and the dihedral angle distribution. The initial structure from the FCM has a broader distribution of $P(R)$ and a higher trans population than that from the BZDM. Since the distribution of $P(R)$ has much influence on the diffusivity and solubility of a small penetrant in a polymer, we checked whether the influence of the initial structures on the distributions of $P(R)$ would remain or not.

During the first 625 ps of MD simulation at 300 K, the influence on the insertion probability and the dihedral angle distribution remained significant. We performed 150 ps of MD runs at 1000 K to relax the structure. Figure 1 shows the time dependence of the dihedral angle distribution of Si–O–Si–O during 150 ps of MD runs at 1000 K. Only the time dependence of the initial 50 ps is shown. Figure 1a shows the time dependence of the dihedral angle distribution with the BZDM parameters and Figure 1b those with the FCM. The dihedral angle distributions decay to the equilibrium values during 20 ps of MD runs at 1000 K. Both structures have the same trans population (~0.4) which are averaged over the last 100 ps of trajectories.

Figure 2 shows the time dependence of the insertion probability $P(R)$ for some values of R during 150 ps of MD runs at 1000 K. Figure 2a shows that of the BZDM and Figure 2b that of the FCM. Although the total free volumes, $P(0)$, of the BZDM and that of the FCM are not different from each other and do not vary with time, the distributions of $P(R)$ are different from each other and vary with time. The free volume distributions, $P(R)$, converged almost completely to the equilibrium values during 20 ps of MD runs at 1000 K. The insertion probabilities averaged over the last 100 ps of trajectories show similar distributions irrespective of the initial structures. Figure 3 shows a plot of $P_m(R)$. $P_m(R)$ of large R decrease with time, and $P_m(R)$ of small R increase with

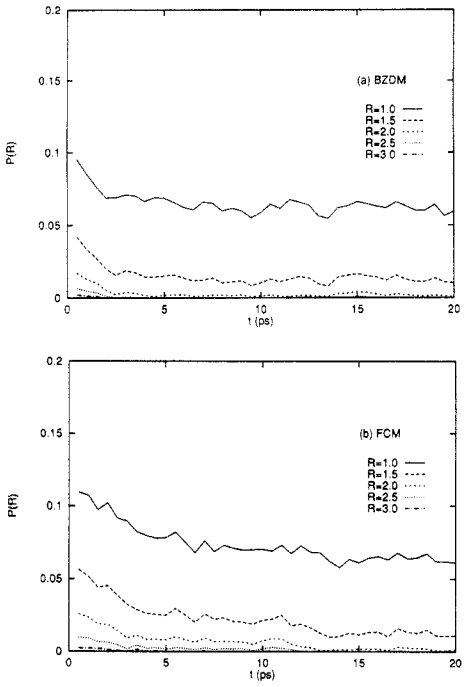

Figure 2. Time dependence of insertion probability $P(R)$ of PDMS for five values of hard-sphere radius R at 1000 K. The initial structures were generated using (a) the BZDM RIS parameters and (b) the FCM.

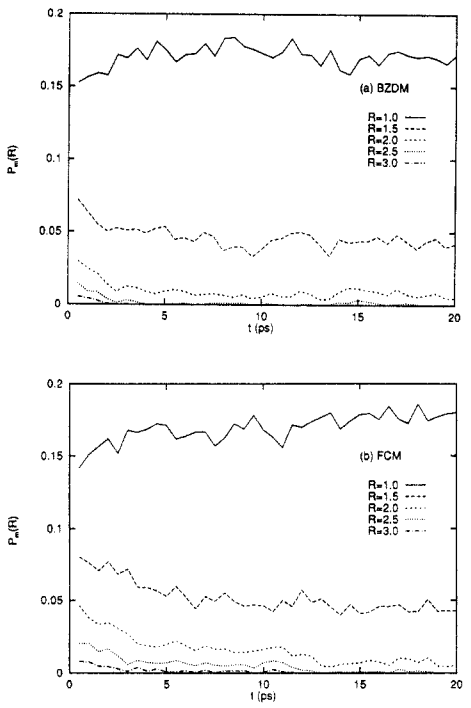

Figure 3. Time dependence of derivative insertion probability $P_m(R)$ of PDMS for five values of hard-sphere radius R at 1000 K. The initial structures were generated using (a) the BZDM RIS parameters and (b) the FCM.

time. This means that large cavities break into small cavities with relaxation of chains. These values come close to equilibrium values during 20 ps.

Because the influence of initial structures on the free volume distribution could be eliminated by the high-temperature MD runs, we use only the structure from the BZDM for the following simulation. We performed 625 ps of MD simulation at 300 K and used the last 500 ps of trajectory for analysis of the amorphous polymer structure. The obtained polymer structure has no long-range order as is evident from the radial distribution function. The

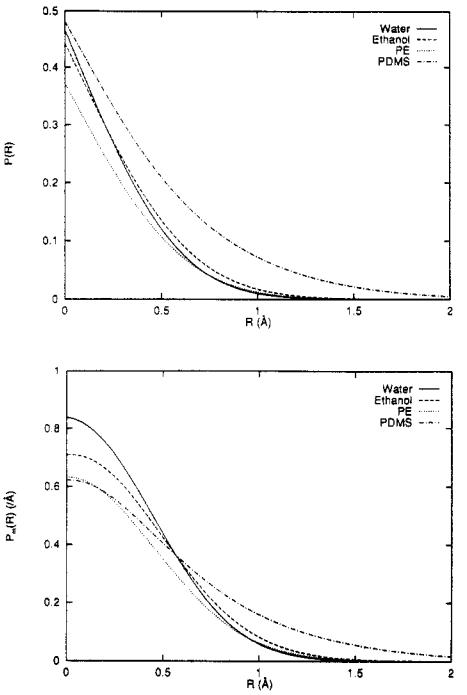

Figure 4. Insertion probabilities $P(R)$ of PDMS, PE, water, and ethanol at 300 K and the derivatives $P_m(R) = -dP(R)/dR$.

dihedral angle distribution was (0.438, 0.275, 0.287) for (t, g^+, g^-) which agreed with the value (0.412, 0.289, 0.299) calculated from the MD trajectory of the oligomer of eight units in vacuum by Bahar et al.[30] The mean-square radius of gyration was 116 Å^2.

Structure of Amorphous PE. After the first 250 ps of MD simulation at 300 K, the trans population of the main chains is approximately 0.7. We examined time dependence of the dihedral angle distribution and the insertion probability at 1000 K. The trans population of dihedral angles relaxed to equilibrium value (0.56) during 3 ps, which is shorter than the time scale of relaxation of the dihedral angle distribution of PDMS. On the contrary, the insertion probability did not vary with time. For PDMS, the initial structure had much influence on $P(R)$. For PE, however, the initial structure had only a little influence on $P(R)$. PDMS has large side groups, $-CH_3$, attached to the main chain, which prevent the main chains from contact. Because bond angles are kept constant in the packing of the chains by the modified self-avoiding random walk, the side group effect is more severe, which leads to the broad distribution of the insertion probability. The rearrangement of the main chains at 1000 K relaxes the free volume distribution. In the case of PE, the rearrangement of the main chains has only a little effect on the insertion probability because PE has no side group.

After 150 ps of the MD run at 1000 K, 1100 ps of MD simulation was performed. The trans population of the main chains relaxed to the equilibrium value (0.71) during 500 ps and fluctuated around this value during the last 600 ps of the MD runs. The dihedral angle distribution calculated from the last 500 ps of trajectory was (0.714, 0.143, 0.143) for (t, g^+, g^-). The mean-square radius of gyration was 334 Å^2.

Insertion Probabilities. Figure 4 shows $P(R)$ and $P_m(R)$ for PDMS, PE, liquid water, and liquid ethanol at 300 K. The free volume fractions, $P(0)$, of PDMS, PE, water, and ethanol were 0.4817, 0.3721, 0.4665, and 0.4425, respectively. The free volume fraction of PDMS is large. PDMS shows a broader distribution of $P(R)$ and $P_m(R)$ compared with the others. The reason for this is that

Table 3. Accessible Volume Fraction of Small Penetrants in Polymers and Liquids at 300 K

penetrant	radius (Å)	$f_v \times 10^4$ [a] in PDMS	in PE	in water	in ethanol
water	1.583	174.89	2.74	1.21	5.84
methane	1.865	77.85	0.22	0.09	0.81
ethanol	2.604	4.16	0.00	0.00	0.00

[a] The accessible volume fraction, which is equal to the insertion probability $P(R)$ for a penetrant of radius R.

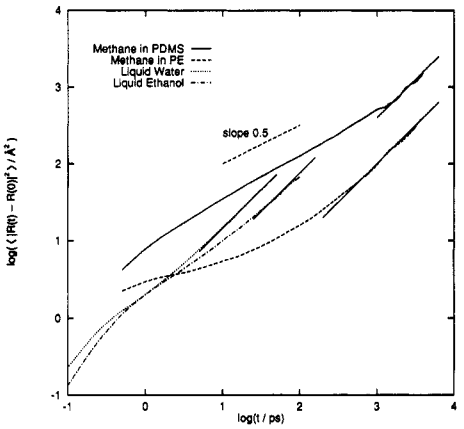

Figure 5. Doubly logarithmic plot of mean-square displacements of methane in PDMS and in PE, pure water, and pure ethanol at 300 K. The straight lines along the data, whose slope is unity, indicate the normal diffusion region.

PDMS has large methyl groups attached to a main chain, which keep neighbor chains apart. Table 3 shows the accessible volume fraction of the penetrant in the polymers and liquids, which is equal to $P(R)$ for the penetrant of radius R. The van der Waals radii, $\sigma/2$, were used for the radii of water and methane, and the kinetic radius,[37] 2.604 Å, was used for the radius of ethanol. The penetrants have a larger accessible volume fraction in PDMS than in PE. The broader free volume distribution will lead to a larger diffusion coefficient and larger solubility of a small penetrant in PDMS.

In spite of restriction by a polymer matrix, experimental diffusion coefficients of methane and water in PDMS are the same order ($\sim 10^{-5}$ cm^2/s) as those of liquid water and ordinary organic liquids. One of the reasons for this is that PDMS has a large free volume fraction and a broad free volume distribution.

Diffusion of Methane in Polymers. We calculated the mean-square displacements from the 5000 ps of trajectories of five methane molecules in PDMS and in PE. The concentrations of methane in PDMS and PE are 0.69 and 0.94 g of solvent/100 g of polymer, respectively. Neither appreciable aggregation nor phase separation was observed in both systems.

Figure 5 shows the mean-square displacements as a doubly logarithmic plot. The results of pure liquid water and ethanol are also plotted. In short time regions, the mean-square displacements follow a power law of t^2. In long time regions, the mean-square displacements are linear in time, where Einstein's equation (eq 9) is applicable. At intermediate regions, anomalous diffusion is observed and the mean-square displacements look like they obey a power law of $t^{0.5}$. The normal diffusion regions of methane in polymers begin at rather long time regions ($\sim$1000 ps for PDMS and $\sim$300 ps for PE) compared with pure liquid water ($\sim$5 ps) and ethanol ($\sim$40 ps), and the anomalous diffusion regions are also longer. Müller-Plathe et al.[8] showed a similar plot for diffusion of helium in polyisobutylene (PIB), where the normal diffusion region

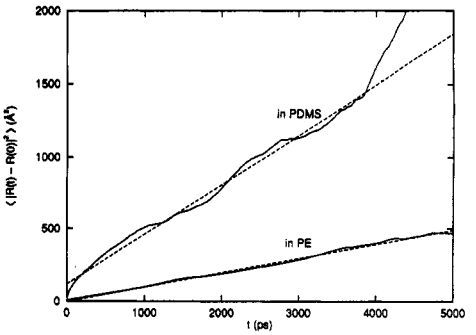

Figure 6. Mean-square displacements of methane in PDMS and PE at 300 K calculated from 5000 ps of trajectories. The straight lines show the least-square fits with the fitting range of the normal diffusion region.

Table 4. Calculated and Experimental Diffusion Coefficients at 300 K

penetrant	matrix	$D \times 10^5$ (cm^2/s) free[a]	aggregate[b]	experiment
methane	PDMS	0.57		2.06[c]
water	PDMS	1.53	0.025	1.45[d]
ethanol	PDMS	0.20	0.005	0.45[d]
methane	PE	0.16		0.045[e]
water	PE	0.78		
ethanol	PE	0.07		
water	water	2.38		2.14[f]
ethanol	ethanol	1.11		1.01[g]

[a] The calculated diffusion coefficients of nonaggregated molecules. [b] The calculated diffusion coefficients of aggregated molecules. The aggregation numbers of water and ethanol in PDMS are 5 and 3, respectively. [c] From measurements on PDMS with 4.9 vol % of a silica filler from ref 39. [d] From the transient permeation experiments at 298 K from ref 38. [e] The average value of diffusion coefficients in ref 10, which are corrected for crystallinity. [f] From ref 40 (298 K). [g] From ref 41 (298 K).

begins about 100 ps. This is the same order as our system of methane in PE. The system of methane in PDMS requires a longer time simulation to obtain the normal diffusion region. It seems that the more complex the system becomes, the longer the anomalous diffusion region extends. If a diffusion coefficient is calculated from a short time scale simulation for a polymer/penetrant system, it will be overestimated.

Figure 6 shows the mean-square displacements. The straight lines show the least-square fits with the fitting ranges of the normal diffusion regions for each system. The calculated values of the diffusion coefficient D in PDMS and PE are 0.57×10^{-5} and 0.16×10^{-5} cm^2/s, respectively. The value in PDMS is rather small compared with the value 2.1 ($\pm$0.8) $\times 10^{-5}$ cm^2/s calculated by Sok et al. about the same system. They calculated the diffusion coefficient from 250 ps of trajectories of two separate runs, which are rather short compared with our calculation. We divided the 5000 ps of trajectory into 20 subsets of 250 ps and calculated the diffusion coefficients from the mean-square displacements of each subset with the fitting range from 10 to 100 ps. This is a situation similar to that of Sok et al. The calculated diffusion coefficient was 1.6 ($\pm$0.6) $\times 10^{-5}$ cm^2/s, which agreed with the result of Sok et al. This value is also the same as the value calculated from the full trajectory with the fitting range of 10–100 ps and was overestimated by about 3 times as large as the value obtained from the normal diffusion region.

Table 4 lists the calculated and experimental diffusion coefficients at 300 K. The diffusion coefficients of liquid water and ethanol are calculated from the trajectories of 50 and 100 ps, respectively. Agreement between the experimental and calculated diffusion coefficients of pure

liquid water and ethanol is fairly good. A MD simulation of approximately 100 ps is sufficient to obtain the diffusion coefficients with high precision for the pure liquid systems. On the other hand, the calculated diffusion coefficient of methane in PDMS is approximately one-fourth of the experimental value and that of methane in PE is approximately 4 times larger than the experimental value which is corrected for crystallinity. We could not expect a completely quantitative agreement for the polymer/penetrant systems even if we use very long time trajectories. Our calculated values, however, agree well with the experiments, considering the fact that different experiments often disagree by a factor of 3 or so for polymer/penetrant systems. The united atom approximation raises the calculated diffusion coefficients of penetrants in polymers, as pointed out by Müller-Plathe et al.[7] for PIB and by Pant et al.[10,11] for PE and PIB; our calculated results for methane in PE is also overestimated. However, the size of the penetrants which we are interested in is large, and the united atom approximation is justified as pointed out by Müller-Plathe et al.[7] Moreover, the discrepancy in our study is the same order as that in PDMS. We expect that the present simulation of the small penetrants in PE and PDMS serves at least as a qualitative comparison for the understanding of the role of polymer–penetrant interaction on the diffusivity.

The diffusion coefficient in PE is about one-fourth that in PDMS. This is a reflection of the narrower distribution of $P(R)$ and $P_m(R)$ in PE than in PDMS.

Diffusion of Water and Ethanol in Polymers. Because water and ethanol tend to form hydrogen bonds in their pure liquids, they may aggregate in a polymer matrix. We performed MD simulation for the systems which contained only one penetrant molecule in the polymer matrix, in order to calculate the diffusion coefficients which were not influenced by aggregation. The concentrations of water and ethanol in PDMS are 0.16 and 0.40 g of solvent/100 g of polymer, respectively, and those in PE are 0.21 and 0.54 g of solvent/100 g of polymer, respectively. MD simulations were performed for 2000 ps.

Figure 7a shows displacements of the penetrant molecules from the initial positions in PDMS and Figure 7b those in PE. The displacements were smoothed over 5 ps in order to reduce the noise level. The displacement of methane is a representative one of the five molecules. The mobility of water is on the same order as methane, and the mobility of ethanol is lower. Both successive small jumps and large jumps are observed. The small penetrants in PDMS have longer jump distances and make more frequent jumps than those in PE. Large vibrational motions of longer time scales are also notable in PDMS.

Figure 8a shows the mean-square displacements of water in PDMS and in PE, and Figure 8b shows those of ethanol. Straight lines show the least-square fits with a fitting range of 50–500 ps. Although the mean-square displacements look linear in time, this time scale is supposed to be within the anomalous diffusion region by contrast with the diffusion of methane in polymers (see Figure 5). Therefore, the diffusion coefficients will probably be overestimated. The calculated values of diffusion coefficients of water in PDMS and in PE are 1.53×10^{-5} and 0.78×10^{-5} cm^2/s, respectively, and those of ethanol are 0.20×10^{-5} and 0.07×10^{-5} cm^2/s, respectively. The diffusion coefficients in PDMS are 2–3 times larger than those in PE. This is a reflection of the broader distribution of $P(R)$ and $P_m(R)$ in PDMS than in PE. The diffusion coefficients of ethanol

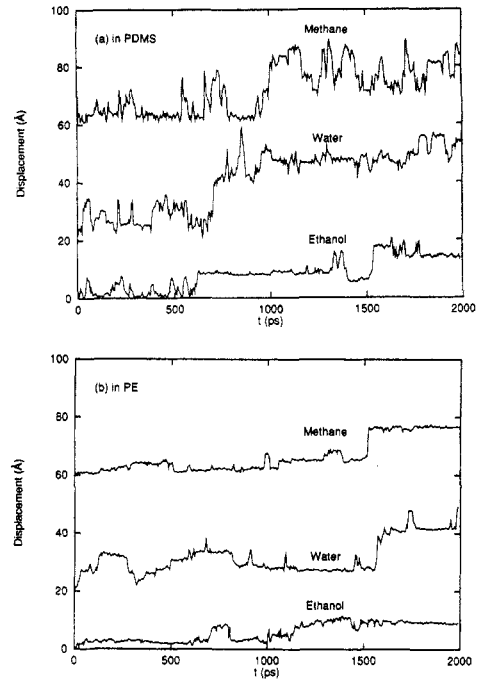

Figure 7. Time-dependence of displacements from the initial positions of methane, water, and ethanol (a) in PDMS and (b) in PE at 300 K. The noise in the original data is smoothed by displaying 5-ps rolling averages. The data for methane and water are offset by 60 and 20 Å, respectively.

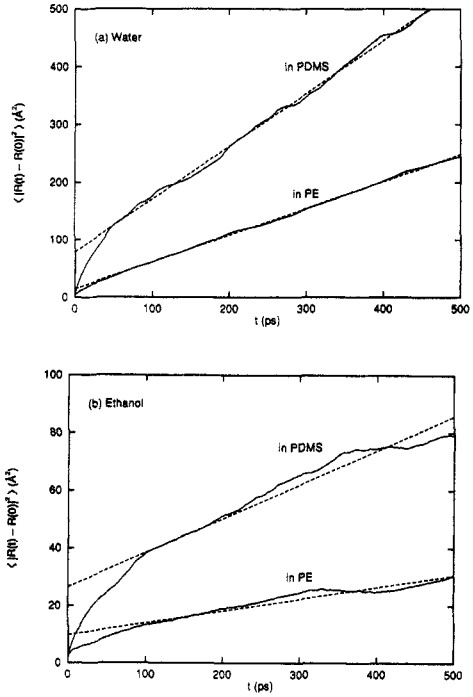

Figure 8. Mean-square displacements of (a) water and (b) ethanol in PDMS and PE at 300 K. Each system contains only one penetrant molecule in the polymers. The straight lines show the least-square fits with a fitting range of 50–500 ps.

are approximately 1 order of magnitude smaller than those of water.

Aggregation of Water and Ethanol in PDMS. In order to analyze aggregative behavior of water and ethanol, we performed two separate runs of MD simulation for the system which contained five penetrant molecules in PDMS. The concentrations of water and ethanol in PDMS are 0.78 and 1.99 g of solvent/100 g of polymer, respectively. The sampling time of long time runs (run 1) was 2000 ps and that of short time runs (run 2) 500 ps. We calculated

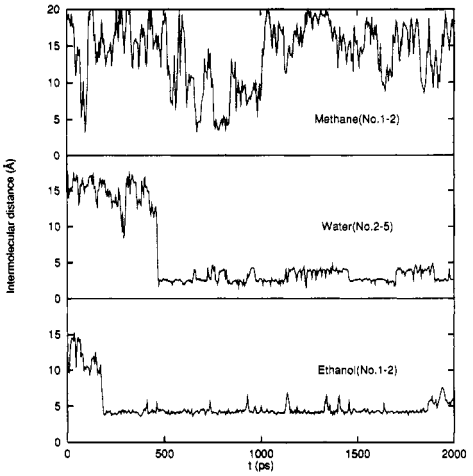

Figure 9. Time dependence of the intermolecular distances of the representative pairs of methane, water, and ethanol in PDMS. The index numbers of the molecules are given in parentheses. The noise in the original data is smoothed by displaying 5-ps rolling averages.

Table 5. Aggregation of Penetrants in PDMS

run[a]	penetrant[b]	t_a (ps)[c]	run[a]	penetrant[b]	t_a (ps)[c]
		Aggregation of Water			
1	1-5	8	2	4-5	10
	3-4	40		1-4-5	89
	1-3-4-5	62		1-3-4-5	478
	1-2-3-4-5	469			
		Aggregation of Ethanol			
1	2-3	6	2	3-4	3
	1-2-3	180		1-5	273

[a] The sampling time of run 1 is 2000 ps (long time runs) and that of run 2 is 500 ps (short time runs). [b] Index number of aggregated penetrant molecules. [c] The time in which the aggregate was formed.

the time dependence of the distances between the centers of mass of the penetrant molecules to confirm the degree of aggregation. Figure 9 shows the time dependence of the representative pair distances of methane, water, and ethanol in PDMS for run 1. For methane, the last 2000 ps of trajectory was used. Methane is not aggregative, as is expected from its liquid properties. Once two molecules approach close together, then they dissociate again. Methane molecules were dispersed uniformly and did not aggregate in the polymer. On the other hand, the molecules of water and ethanol interact so strongly with each other that they form aggregates. Once forming the aggregates, they did not dissociate to the single molecules.

Table 5 shows the index number of molecules which form aggregates and the time t_a when the aggregates are formed. Water molecules were dimerized in PDMS, and the aggregates grow further to the larger aggregates of four or five molecules. Ethanol molecules also form aggregates of two or three molecules. Between runs 1 and 2, the qualitatively same aggregative profiles are reproduced. Pure water aggregates more strongly than pure ethanol, as conjectured by the respective boiling points or the heats of vaporization. This effect is carried over to the polymer/penetrant system, since the OPLS and SPC/E force field parameters are adjusted to reproduce the experimental heats of vaporization. On the other hand, ethanol interacts more favorably with the hydrophobic polymer than water. In the PDMS membrane, the aggregate of water is thermodynamically more stable than that of ethanol. Moreover, water has a larger diffusivity than ethanol. Therefore, water has the higher probability which two molecules encounter in PDMS and forms more aggregates than ethanol.

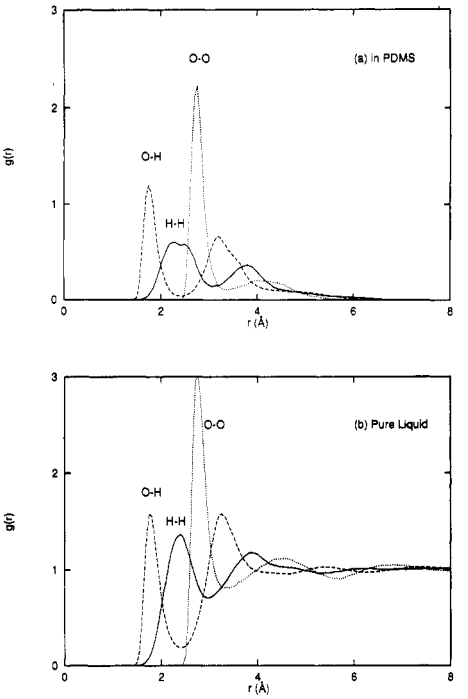

Figure 10. Radial distribution functions $g(r)$ of water at 300 K (a) in PDMS and (b) in liquid water. The $g(r)$ in PDMS is normalized by the number density in liquid water.

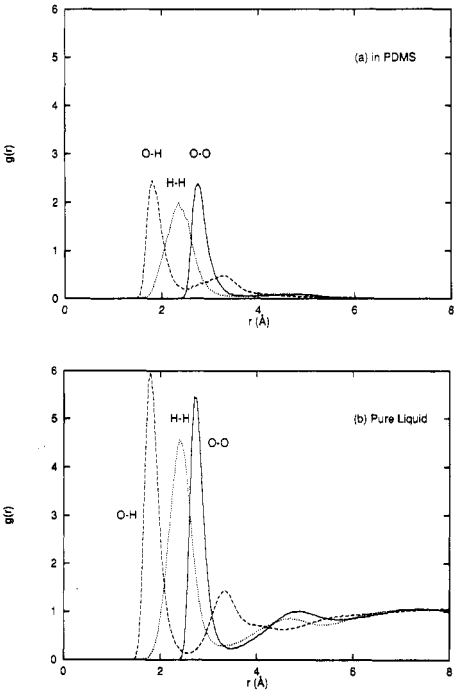

Figure 11. Radial distribution functions $g(r)$ of ethanol at 300 K (a) in PDMS and (b) in liquid ethanol. The $g(r)$ in PDMS is normalized by the number density in liquid ethanol.

We calculated radial distribution functions of small penetrants in PDMS and in the pure liquids. The radial distribution function of methane shows no significant peak. On the other hand, the radial distribution functions of water and ethanol have some significant peaks due to the aggregation. Figures 10 and 11 show the results of water and ethanol, respectively. Part a of each figure shows the results in PDMS and part b of each figure those in the pure liquids. The radial distribution functions in PDMS are normalized by the number densities of the pure liquids. The first and second peaks of the radial distribution functions in PDMS appeared at the exact same radial distances as those in the pure liquids. The hydrogen-

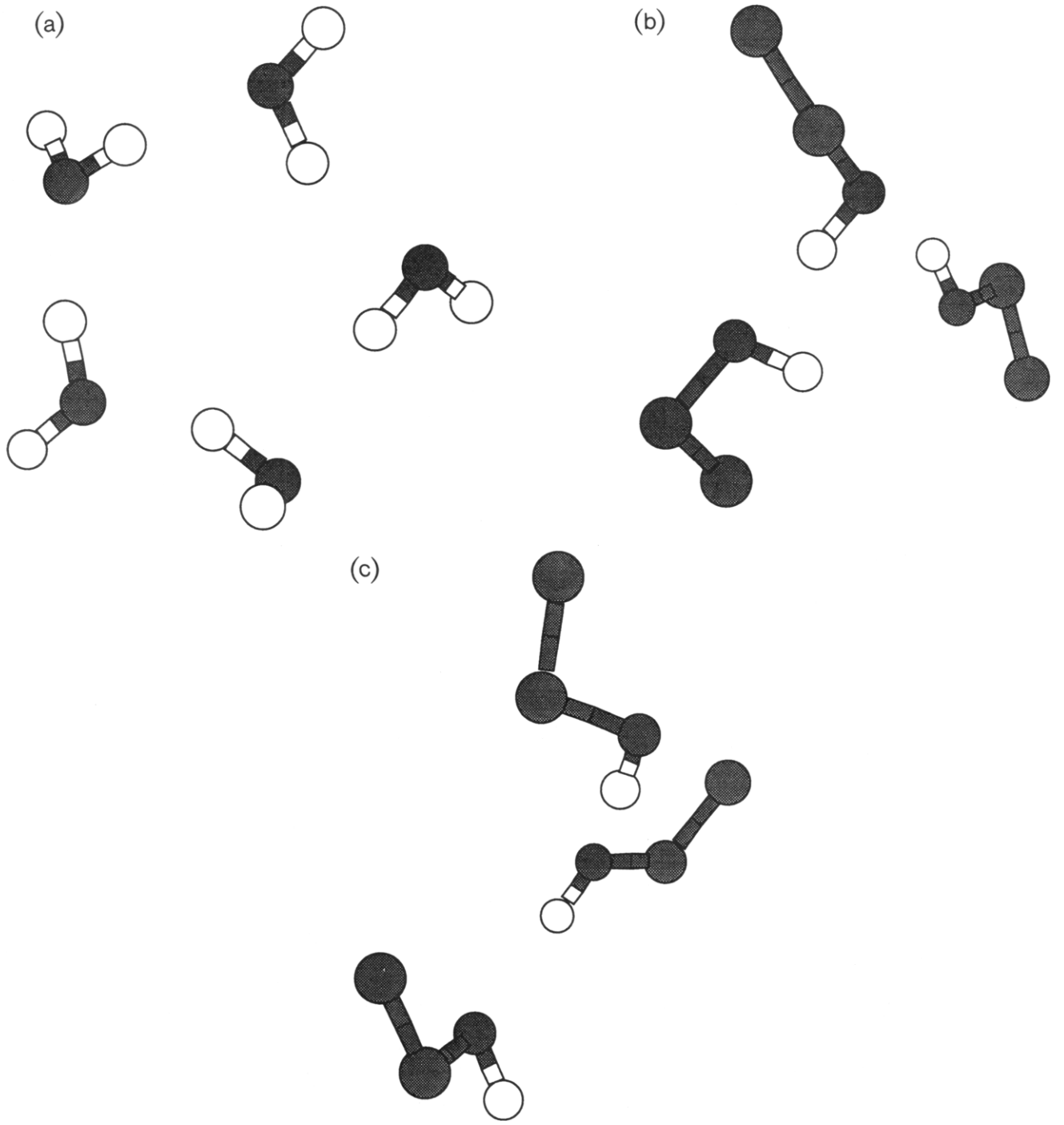

Figure 12. Snapshots of aggregated molecules in PDMS: (a) water, (b) cyclic ethanol molecules, and (c) linear ethanol molecules. Open circles indicate hydrogen atoms.

bonded structures of the aggregates are supposed to be similar to the those in the pure liquids.

We made the animations of aggregates of water and ethanol in PDMS. Figure 12 shows the snapshots. We found that the aggregate of the five water molecules formed a cyclic structure (a), instead of linearly bonded molecules. For the aggregate of the three ethanol molecules, the hydroxyl groups face each other by strong hydrogen bonds, and ethyl groups of ethanol dangled around the center. The structure of the center exchanged between a cyclic one (b) and a linear one (c).

Diffusion coefficients will be affected by the degree of aggregation. We calculated the diffusion coefficients from the trajectories of aggregated penetrant molecules in the long time runs. The aggregation numbers are 5 and 3, the sampling times were 1500 and 1850 ps, and the calculated diffusion coefficients were 2.5×10^{-7} and 0.5×10^{-7} cm^2/s for water and ethanol, respectively. The results are listed in Table 4. The diffusion coefficients were decreased to about one-fiftieth by aggregation. The values are very small. We examined the trajectories and displacements from initial positions of the aggregated penetrant molecules in PDMS. The cooperative jump motions of small molecules in the cluster are found in the plots. The motions of the molecules in the aggregate are not the translational diffusion of the whole cluster but the exchange of the penetrant molecules within the same cluster. The diffusion coefficients of the aggregated molecules are virtually zero compared with that of the free molecules.

Comparison with Experiment. Table 4 lists the calculated and experimental diffusion coefficients at 300

K. The aggregation numbers of water and ethanol in PDMS are 5 and 3, respectively. The experimental diffusion coefficients D of water and ethanol in PDMS were determined by Okamoto et al.[38] from the transient permeation experiments for pure components and also for 10 and 30 wt % ethanol solutions. These values agreed with the concentration-averaged diffusion coefficients $\bar{D}$ which Okamoto et al. determined from sorption and pervaporation experiments for water/ethanol mixtures in PDMS. The membrane used in the experiment is press-cured pure PDMS, whose density is 0.974 g/cm^3, and is slightly higher than our system. The higher density and the press cure reduce the diffusion coefficients. Our calculated values of diffusion coefficients are supposed to be determined from the anomalous diffusion region, which leads to overestimated diffusion coefficients. Although the condition is slightly different between our calculation and their experiment, we can conclude that the experimental diffusion coefficients are greater than our calculated values of aggregated molecules; the experimental values are closer to the calculated diffusion coefficients of nonaggregated molecules. Taking account of different conditions, the experimental values are slightly larger than the calculated values of nonaggregated molecules.

In the pervaporation experiments, the concentration of the penetrants decreases monotonically from the feed side of the membrane to the permeate side. The aggregation is supposed to have some effect on the diffusion process in the feed side of the membrane but only a little effect on the diffusion in the permeate side or middle of the membrane. Okamoto et al.[38] determined the solubilities of the various concentrations of aqueous solutions of ethanol in PDMS membranes by sorption experiments. Only a small amount of water is dissolved in the PDMS membrane, and there is no experimental value about solubility of pure water. The extrapolated value to the zero concentration is much lower than 0.1 g of solvent/100 g of polymer, which is lower than the concentration of water (0.78) in our system of five water molecules in PDMS. On the other hand, the solubility of pure ethanol in PDMS is 7.45 g of solvent/100 g of polymer, which is higher than the concentration of our system (1.99). Therefore, the effect of aggregation is important for pure ethanol, especially on the feed side of the membrane. At this concentration, the effect of relaxation of the PDMS chains by ethanol is also important. Although the former effect decreases the diffusion coefficient, the latter effect increases it. At the intermediate concentration ($\sim$50 wt %) of the aqueous solution of ethanol, which is the usual case for pervaporation using a PDMS membrane, the experimental solubility of ethanol is about 0.5 g of solvent/100 g of polymer, which is lower than the concentration of our system. This order of solubility, however, does not assure that the aggregation of penetrants is not formed.

It is generally known that clustering of water molecules in polymers is allowed in usual experiments. The solubility of pure water in PDMS is very low. When polymer chains are relaxed by ethanol molecules, however, water molecules are soluble in some regions of the membrane, the regions where clusters of water are formed and grow. The diffusion coefficient of aggregated penetrants is virtually zero, as shown in our simulation. The fact that the experimental diffusion coefficient is so much closer to the value for free molecules is explained as follows. The penetrants form clusters in suitable holes in the polymer, where they are immobilized. Once all the holes are filled, any additional penetrant can be regarded as free, and only free penetrants contribute appreciably to the overall transport.

This aspect agreed with the experiments of Okamoto et al.[38] In their experiments, the concentration-averaged diffusion coefficients $\bar{D}$ for each component, which are determined from pervaporation, were independent of the feed composition. The values of D for each component, which are determined from the transient permeation experiments for the vapor of pure components, were in fairly good agreement with the values of $\bar{D}$. Moreover, the values of D for water and ethanol, which are determined from the transient permeation experiments for 10 and 30 wt % ethanol solutions, were the same as the values for pure components. The experimental results led to the conclusion that water and ethanol molecules permeate separately in the membrane as isolated molecules.[38] Our calculated result supports this view.

Our calculated values for nonaggregated penetrant molecules are in good agreement with the experimental values. Taking the difference of the conditions between the simulation and the experiment into consideration, the calculated values tend to be lower than the experiments. The average pressure, which is calculated on an atomic basis for the system of a ethanol molecule in PDMS, is negative several tens MPa. The negative pressure leads to an overestimate of the diffusion coefficients for very small penetrants. For comparatively large penetrant molecules and clusters, however, the restriction of constant volume and constant shape of the unit cell, which was used in our simulation, may reduce the diffusivity by suppressing the motion of large free holes. For the system of ethanol in PDMS, the relaxation effect of polymer chains by ethanol molecules, which is observed in the experiment, raises the diffusivity. This effect may not be sufficiently included in this simulation.

Conclusion

The larger free volume and broader free volume distribution of PDMS result in the 3 times higher diffusion coefficients of methane, water, and ethanol in PDMS than in amorphous PE. Although there are some difficulties in obtaining quantitative agreement, the calculated diffusion coefficients of the nonaggregated penetrant molecules agree reasonably with the experiments. Since water and ethanol have aggregative nature, they form aggregates in PDMS on our MD simulations for the systems which contain more than a single penetrant in the unit cell. The hydrogen-bonded structures of the aggregates are similar to those in the pure liquids. The calculated diffusion coefficients of aggregated molecules in PDMS are virtually zero, and those of free molecules are close to the experiments. This implies that the overall transport is ascribed to diffusion of free penetrants.

In this paper, the diffusional motion of small penetrants was detected by the mean-square displacement and by the displacement of penetrants and was linked to the static property of polymers, the insertion probability. The mechanism of the diffusion process was, however, not fully elucidated. The diffusion of small penetrants is connected with the dynamics of polymer chains. Cooperative motion is very important especially for the system of large penetrants which have internal degrees of freedom, or polar penetrants in polymers. The mechanism of diffusion will be treated in an upcoming paper.

Ethanol has a smaller diffusion coefficient than water in PDMS but has a larger permeation rate. The reason for this is that ethanol has a larger solubility than water. It is necessary to examine solubility in terms of various components such as free volume and the interaction potential for comprehension of the permeation phenomena

of small penetrants in the membranes. We will analyze the solubility of small molecules in polymers in an upcoming paper.

Acknowledgment. Generous amounts of computer time were provided by the Supercomputer Laboratory, Institute for Chemical Research, Kyoto University. Computer time was provided also by Computer Center, Institute for Molecular Science.

References and Notes

(1) Huang, R. Y. M., Ed. *Pervaporation Membrane Separation Processes*; Elsevier Science Publishers B. V.: Amsterdam, The Netherlands, 1991.
(2) Widom, B. *J. Chem. Phys.* **1963**, *39*, 2808.
(3) Takeuchi, H.; Okazaki, K. *J. Chem. Phys.* **1990**, *92*, 5643.
(4) Takeuchi, H. *J. Chem. Phys.* **1990**, *93*, 2062.
(5) Sok, R. M.; Berendsen, H. J. C.; van Gunsteren, W. F. *J. Chem. Phys.* **1992**, *96*, 4699.
(6) Müller-Plathe, F. *J. Chem. Phys.* **1992**, *96*, 3200.
(7) Müller-Plathe, F.; Rogers, S. C.; van Gunsteren, W. F. *Macromolecules* **1992**, *25*, 6722.
(8) Müller-Plathe, F.; Rogers, S. C.; van Gunsteren, W. F. *Chem. Phys. Lett.* **1992**, *199*, 237.
(9) Müller-Plathe, F.; Rogers, S. C.; van Gunsteren, W. F. *J. Chem. Phys.* **1993**, *98*, 9895.
(10) Pant, P. V. K.; Boyd, R. H. *Macromolecules* **1992**, *25*, 494.
(11) Pant, P. V. K.; Boyd, R. H. *Macromolecules* **1993**, *26*, 679.
(12) Gusev, A. A.; Arizzi, S.; Suter, U. W.; Moll, D. J. *J. Chem. Phys.* **1993**, *99*, 2221.
(13) Gusev, A. A.; Suter, U. W. *J. Chem. Phys.* **1993**, *99*, 2228.
(14) Shah, V. M.; Stern, S. A.; Ludovice, P. J. *Macromolecules* **1989**, *22*, 4660.
(15) Arizzi, S.; Mott, P. H.; Suter, U. W. *J. Polym. Sci., Polym. Phys. Ed.* **1992**, *30*, 415.
(16) Greenfield, M. L.; Theodorou, D. N. *Macromolecules* **1993**, *26*, 5461.
(17) Misra, S.; Mattice, W. L. *Macromolecules* **1993**, *26*, 7274.
(18) Pratt, L. R.; Pohorille, A. *Proc. Natl. Acad. Sci. U.S.A.* **1992**, *89*, 2995.
(19) Eisenberg, D.; Kauzmann, W. *The Structure and Properties of Water*; Oxford University Press: London, U.K., 1969.
(20) Jorgensen, W. L. *J. Phys. Chem.* **1986**, *90*, 1276.
(21) Zoller, P. *J. Appl. Polym. Sci.* **1979**, *23*, 1051.
(22) Jorgensen, W. L.; Madura, J. D.; Swenson, C. J. *J. Am. Chem. Soc.* **1984**, *106*, 6638.
(23) Weiner, S. J.; Kollman, P. A.; Case, D. A.; Singh, U. C.; Ghio, C.; Alagona, G.; Profeta, S.; Weiner, P. *J. Am. Chem. Soc.* **1984**, *106*, 765.
(24) Jorgensen, W. L.; Tirado-Rives, J. *J. Am. Chem. Soc.* **1988**, *110*, 1657.
(25) Berendsen, H. J. C.; Grigera, J. R.; Straatsma, T. P. *J. Phys. Chem.* **1987**, *91*, 6269.
(26) Ryckaert, J. P.; Ciccotti, G.; Berendsen, H. J. C. *J. Comput. Phys.* **1977**, *23*, 327.
(27) Clarke, J. H. R.; Brown, D. *Mol. Simul.* **1989**, *3*, 27.
(28) Flory, P. J. *Statistical Mechanics of Chain Molecules*; Interscience: New York, 1969.
(29) Flory, P. J.; Crescenzi, V.; Mark, J. E. *J. Am. Chem. Soc.* **1964**, *86*, 146.
(30) Bahar, I.; Zuniga, I.; Dodge, R.; Mattice, W. L. *Macromolecules* **1991**, *24*, 2986.
(31) Bahar, I.; Zuniga, I.; Dodge, R.; Mattice, W. L. *Macromolecules* **1991**, *24*, 2993.
(32) Verlet, L. *Phys. Rev.* **1967**, *159*, 98.
(33) Allen, M. P.; Tildesley, D. J. *Computer Simulation of Liquids*; Oxford University Press: Oxford, U.K., 1987.
(34) Nosé, S. *J. Chem. Phys.* **1984**, *81*, 511.
(35) Ferrario, M.; Ryckaert, J. P. *Mol. Phys.* **1985**, *54*, 587.
(36) Palmer, B. J.; Garrett, B. C. *J. Chem. Phys.* **1993**, *98*, 4047.
(37) Loyd, D. R.; Meluch, T. B. *ACS Symp. Ser.* **1985**, *269*, 47.
(38) Okamoto, K.; Nishioka, S.; Tsuru, S.; Sasaki, S.; Tanaka, K.; Kita, H. *Kobunshi Ronbunshu* **1988**, *45*, 993.
(39) Stern, S. A.; Shah, V. M.; Hardy, B. J. *J. Polym. Sci., Polym. Phys. Ed.* **1987**, *25*, 1263.
(40) Wang, J. H. *J. Am. Chem. Soc.* **1951**, *73*, 510.
(41) Rathbun, R. E.; Babb, A. L. *J. Phys. Chem.* **1961**, *65*, 1072.